hep-ph/9402345, TIFR/TH/93-57, BU-TH-93/5

High Precision J/ψ and Υ-production data and the Nuclear Glue

R.V. Gavai*

Theory Group, Tata Institute of Fundamental Research, Bombay 400 005, India

R.M. Godbole†

Dept. of Physics, Univ. of Bombay, Vidyanagari, Bombay 400 098, India

Abstract

We use the high statistics E-772 data on the nuclear dependence of the production of quarkonia (J/ψ and Υ) and dimuons at large transverse momentum (p_T) in p-A collisions to get information about the gluonic EMC effect. We find a satisfactory quantitative agreement of the theoretical predictions with the data although none of the models of the EMC effect we consider could account for the entire data. Since all the qualitative features are understood none the less in terms of perturbative QCD with nuclear dependent parton densities, our results suggest that these data can now be used for a better determination of the nuclear parton densities. Our conslusions are shown to be insensitive to the hadronisation mechanism for the quarkonia.

PACS numbers: 12.38 Bx, 12.38 Mh, 13.85 Ni, 13.85 Qk

*E-mail: gavai@theory.tifr.res.in

†E-mail: rohini@theory.tifr.res.in

I. INTRODUCTION

The observation of a nontrivial nuclear dependence of the parton densities, the EMC effect [1], confirmed later in a further series of deep inelastic scattering experiments [2], still lacks a clear theoretical understanding even after a decade. A large variety of models [2], with widely differing basic underlying physics mechanisms, have been proposed to explain the EMC effect. In all of these, some model parameters have to be fitted to reproduce the measured ratio ρ of the structure function ${F_2}^A$ (per nucleon) for the nucleus to that of the nucleon ${F_2}^p$. As a result, the nuclear quark densities are very similar in all these models. However, their predictions for nuclear gluon densities are quite different. Hence a good measurement of the gluonic ratio,

$$\rho_g = \frac{g^A(x,Q^2)}{Ag^P(x,Q^2)}$$

can play an important role in distinguishing the different models of EMC effect. This information can be obtained by studying the nuclear dependence of different hard scattering processes [3] such as jet production [4], direct photon production [5], quarkonium (J/ψ and Υ) production [6,7,9,10], $\mu^+\mu^-$ pair production [11] with nuclear targets. Recently the associated production of J/ψ and a photon at large p_T has also been suggested [12] as a means to catch a glimpse of the gluonic EMC effect and to help unravel the correct model of EMC effect.

Nuclear dependence of quarkonium and $\mu^+\mu^-$ pair production can be very crucial for the various experimental signals of the formation of Quark-Gluon Plasma (QGP) in relativistic heavy ion collisions. It has been suggested [13] that due to formation of QGP, the J/ψ production in A-A collisions will be suppressed and the suppression is expected to exhibit a characteristic p_T-dependence with a maximum suppression at $p_T = 0$ [14]. To analyse the feasibility of using this suppression as a signal for QGP formation it is, however, necessary to understand clearly the expectations of perturbative quantum chromodynamics, (pQCD), for the quarkonia production in A-A collisions. The observation of a p_T-dependent J/ψ-suppression by the NA38 experiment [15] further made such a study of pQCD imperative.

The applicability of pQCD for this process is justified because of the short time scale for the production of a heavy quark-antiquark ($Q\bar{Q}$) pair which is $O(1/2M_Q)$ for a heavy quark of mass M_Q. In the pQCD approach the initial state dependence of J/ψ or Υ production comes through the nuclear parton densities. Earlier investigations [6,16] have revealed that the nuclear dependence of parton densities gives rise to a J/ψ-suppression in A-A and p-A collisions which is qualitatively similar to the proposed QGP signature. Since any suppression due to QGP formation or a hot dense hadron gas amounts merely to a change in the hadronisation model and/or final state interactions, it is clear that a critical assessment of the utility of J/ψ-suppression as a signal for QGP formation needs a good understanding of nuclear parton densities. Since quarkonia are usually detected through their $\mu^+\mu^-$ decay, the continuum $\mu^+\mu^-$ pair production in A-A collisions has to be investigated as well. Fortunately, high statistics data on J/ψ or Υ and $\mu^+\mu^-$ pair production with nuclear targets [17–19] has recently become available from the Fermilab E772 experiment. In this paper we compute large-p_T $J/\psi, \Upsilon$ and dimuon production in p-A collisions in pQCD and compare it with the E772 data with a view to get a handle on the gluonic EMC effect. The main advantage of comparing the model predictions with all these data from the same experiment is of course in minimizing the effects of systematic uncertainties. We consider the processes

$$p + A \to J/\psi(\Upsilon, \mu^+\mu^-) + X$$

as due to a hard collision between partons from the proton and the nuclear target with mass number A. The nuclear dependence is incorporated only through the parton densities which is where the different models of EMC effect come into picture. The hard scattering cross-sections for $Q\bar{Q}$ production ($Q = c$ (b) for $J/\psi(\Upsilon)$) and $\mu^+\mu^-$ pair production are available in literature [20–22]. Two different hadronisation models [23,24] exist in the literature for the hadronisation of the $Q\bar{Q}$ pair into a quarkonium. In our work we use both of them to assess the uncertainty in our results due to these. Earlier an attempt [9] was made to extract the nuclear glue from the E772 data by using the approximation of gluon dominance of the partons in the initial state and by assuming that the $Q\bar{Q}$ production takes place at $p_T = 0$

for the pair. We comment on the reliability of this approach.

The plan of the paper is as follows: in the next section we summarize different theoretical models for nuclear parton densities (i.e. the EMC effect) which we use. In section III, we first present the details of the theoretical formalism we use to calculate the quarkonia production at large-p_T. We then discuss and compare the two hadronisation models we employ and point out the major kinematical differences in the two models. Following this the limitations of the gluon dominance approximation, used in Ref. [9] to extract ρ_g from J/ψ and Υ production are highlighted. Finally, we end the section by presenting a comparison of our pQCD calculations with the data from the E772 experiment for the J/ψ and Υ–production at large p_T. The theoretical predictions are obtained for the different nuclear parton densities by imposing the experimental cuts of the E772 group on the ranges of the kinematical variables. We also compare the predictions of different hadronisation models with each other. In the next section, we discuss the formalism for calculating the background, continuum $\mu^+\mu^-$ pair production at large-p_T and present our results for the ratio of partially integrated cross-sections of dimuon production for different nuclear targets and parton densities and compare them with the E772 data. We then present our conclusions in the last section.

II. MODELS FOR NUCLEAR PARTON DENSITIES

We define the nuclear parton densities by removing a factor A, where A is the atomic number of the nucleus, so that the cross section defined below is per nucleon of the target, making it directly comparable to the pp case. The presence of the EMC-effect tells us that the nuclear parton densities are different from those of a nucleon even after this rescaling, i.e., the ratio ρ, defined in the introduction, is a nontrivial function of x, where x is fraction of the momentum of a *nucleon* which the parton carries: $0 \leq x \leq A$ for the nucleus. There are many models in the literature which predict ρ in terms of some parameters which can be fixed by comparing with the data on the EMC-effect. The corresponding ρ_g is then usually predicted in these models. We limit the scope of our present investigations by concentrating

on three different models, which are chosen as typical examples of sets of models based on similar physical concepts: i) the gas model [25], ii) the rescaling model [26] and iii) the six-quark cluster model [27]. In all the three cases, we neglect QCD-evolution, since such corrections are small in the kinematic range of interest to us. Fig. 1 displays the predicted ρ_g for all these three models. The details of these predictions are given below for each of the model.

A. The Gas Model

The parton densities of a nucleus with atomic number A are defined in the Gas model [25] as a sum of two components.

$$f_{i/A}(x) = (1-\omega)\tilde{f}_{i/N}(x) + \frac{1}{A}\sum_{r=1}^{A}\omega^r(1-\omega)^{A-r} f_{i,r}^{\rm gas}(x;\mu,T) \tag{1}$$

The first term, occuring with a weight $(1-\omega)$, is that for a free nucleon parton density after corrections for its Fermi motion inside the nucleus. The second component is written in terms of thermal distributions of momenta at a temperature T, leading to the following functions $f_r^{\rm gas}(x;\mu,T)$:

$$f_{q,r}^{\rm gas}(x;\mu,T) = \frac{2r_0^3T^3}{\pi}\left[\phi\ \ell n(1+ze^{-\phi}) + \frac{1}{2}\ell n^2(1+ze^{-\phi}) + Li_2\Big(\frac{z}{z+e^{\phi}}\Big)\right] \tag{2}$$

and

$$f_{g,r}^{\rm gas}(x;\mu,T) = \frac{2r_0^3T^3}{\pi}\Big[Li_2(e^{-\phi}) - \phi\ \ell n(1-e^{-\phi})\Big] \tag{3}$$

Here $r_0 = 1.2$ fm, $\phi = Mx/2T$, $z = \exp(-\mu/T)$, where M is the nucleon mass and $Li_2(x)$ is the Euler dilogarithm function. Using the constraint on the total baryon number of the nucleus to eliminate the chemical potential μ, one has two model parameters, T and ω, for each nucleus.

Using the CDHS parametrisations [28],

$$
\begin{aligned}
F_2^{\nu p}(x) &= 1.1(1+3.7x)(1-x)^{3.9} \\
x\sigma_p(x) &= 0.17(1-x)^{8.54} \\
xf_{g/p}(x) &= 2.62(1+3.5x)(1-x)^{5.9}
\end{aligned}
\tag{4}
$$

for $F_2^p(x)$ (here $\sigma_p(x)$ is the total sea density) and the data on $\rho(x) = F_2^A(x)/AF_2^p(x)$ these parameters have been fixed [25] for many nuclei, including the ones used for the E772 experiment. The corresponding $\rho_g(x)$ is then predicted uniquely. We summarise them in Table I. It may be mentioned here that using a different set of structure functions for proton instead of eq. (4) necessitates a time-consuming re-analysis of the EMC-data to obtain T and ω. For this reason we have not used more recent parametrisations for the proton structure function and we are also constrained to use *different* proton structure functions in different models.

B. The Rescaling Model

Scaling models [26,29,30] seek to explain the EMC effect as arising from the change in the QCD-scale in going from a nucleon to a nucleus. The nuclear parton densities at a scale Q^2 are obtained from the parton densities in a proton at the same Q^2 by evolving them to a scale $\xi_A Q^2$, i.e., the nuclear parton density per nucleon $f_{i/A}(r, Q^2)$ is given by

$$
f_{i/A}(x, Q^2) = f_{i/p}(x, \xi_A Q^2) \tag{5}
$$

In this paper, we use the rescaled nuclear densities as obtained in Refs. [29,30] where $\xi_A = A^{2/3}$ and the starting nucleon parton densitites were taken [30] to be a parameterisation of the EMC Deuterium data at $Q^2 = 20$ GeV^2. For further details, we refer the reader to Ref. [30].

C. The six-quark cluster model

The six-quark cluster model [27] is also a representative of the two-component models for EMC effect. In this model, it is assumed that when two nucleons get closer to each other than a certain critical radius they merge together to form a six-quark cluster. By assuming the probability to form higher clusters to be negligible, the remaining model inputs are the probability of forming such a cluster and the form of the parton distributions in the 3-quark and 6-quark clusters. The latter are chosen using the quark-counting rules and the constraints of i) normalization of valence densities (an N-quark cluster has N valence quarks), and ii) conservation of momentum. It is further assumed that the average momentum carried by the sea partons is the same for the three- and six-quark clusters and that it is ~ 0.2 of that of the gluons. The forms of nuclear densities per nucleon in this model are,

$$f_{i/A}(x) = (1-\epsilon) f_{i,3}(x) + \frac{\epsilon}{2} f_{i,6}\left(\frac{x}{2}\right) \quad , \tag{6}$$

where ϵ is the probability to find a six quark cluster which increases with A [31] and the subscripts denote the cluster size. The values of ϵ which we used are given in Table I. Specific choices [27] for the valence density $V(x) = f_{u_V}(x) + f_{d_V}(x)$, sea density $S(x)$ and the gluon $G(x)$ for an N quark cluster ($N = 3, 6$), which we used in our analysis presented here, are given by

$$\begin{aligned} xV_N(x) &= N x^{0.5}(1-x)^{2N-3} \Big/ B\left(\frac{1}{2},\ 2N-2\right) \\ xS_N(x) &= \frac{N-1}{2(4N-3)}\ (a_N+1)\ (1-x)^{a_N} \\ xf_{g,N}(x) \equiv xG_N(x) &= \frac{5(N-1)}{2(4N-3)}\ (c_N+1)\ (1-x)^{c_N} \quad , \end{aligned} \tag{7}$$

with $a_3 = 9,\ a_6 = 11,\ \ c_3 = 7$, and $c_6 = 10$ [11]. Here B is the usual Euler function and $S_N(x)$ represents the sum of sea quark densities over all flavours. With a further assumption of $\bar{f}_{\bar{s},N}(x) = \frac{1}{2}\ f_{\bar{u},N}(x) = \frac{1}{2}\ f_{\bar{d},N}(x)$, the $\bar{u}$ distribution for the N-quark cluster is given by $f_{\bar{u},N}(x) = \frac{1}{5}\ S_N(x)$.

III. THEORETICAL FORMALISM

The problem of heavy quark-antiquark pair ($Q\bar{Q}$) production has been studied extensively both experimentally and theoretically. In the pQCD approach the quarkonium production cross-section can be calculated by convoluting the hard scattering subprocess cross-section (at a give order in α_s) with the appropriate initial parton densities and suitably chosen hadronization functions. Two popular hadronisation models which describe conversion of the $Q\bar{Q}$ pair into quarkonia are i) the semilocal-duality (SL) model and ii) the colour singlet (CS) model. Since we employ both of them in our work, we will discuss them briefly below. As we shall see, the differences in their details result in different kinematics for the same process at formally the same order of perturbation theory. It is therefore interesting to compare their predictions with the E772 data to check the robustness of the pQCD approach; any differences are likely to provide a clue on the hadronisation of the ($Q\bar{Q}$)-pair.

A. Semilocal Duality Model

In this model one first computes the basic $Q\bar{Q}$ production cross-section. The quarkonium cross-section is then obtained by simply restricting the invariant mass of the $Q\bar{Q}$ pair between $2M_Q$ and $2M_{h_Q}$ (where M_Q is the heavy quark mass and M_{h_Q} is the mass of lowest lying q-flavoured meson) and by multiplying the cross-section by a constant. The underlying assumption is that irrespective of its invariant mass the ($Q\bar{Q}$)-pair is equally likely to turn in to a given quarkonium provided it is below the threshold of the heavy flavoured mesons. The constant *may* depend on the colliding energy. However, we will need to consider only ratios of cross-sections for the nucleon and nuclear target at a fixed energy, and the constant drops out of such ratios. The $Q\bar{Q}$ cross-section itself is given by,

$$\sigma(pA \to Q\bar{Q}X) = \sum_{p_1,p_2} \int_{\frac{4M_Q^2}{s}}^1 dx_1 \int_{\frac{4M_Q^2}{sx_1}}^1 dx_2 \Big[f_{p_1/p}(x_1) f_{p_2/A}(x_2) + f_{p_2/p}(x_1) f_{p_1/A}(x_2) \Big] \hat{\sigma}_{p_1 p_2}(\hat{s}, M_Q^2) \tag{8}$$

Here $f_{p/h}(x)$ is the parton density for parton p in hadron h, x is the momentum fraction of h carried by p and $\hat{\sigma}$ is the appropriate subprocess cross-section integrated over all the subprocess variables. The square of the total centre of mass (cm) energy of the partonic system is given by

$$\hat{s} = sx_1x_2$$

where s is the square of the cm energy of the p-A system.

For $Q\bar{Q}$ production both the $O(\alpha_s^2)$ [20] and $O(\alpha_s^3)$ [21] expressions for $\hat{\sigma}$ are available. The subprocesses which contribute at $O(\alpha_s^2)$ are

$$gg \to Q\bar{Q}, \quad q\bar{q} \to Q\bar{Q} \tag{9}$$

and the ones contributing at $O(\alpha_s^3)$ are

$$gg \to Q\bar{Q}g, \quad q\bar{q} \to Q\bar{Q}g, \quad qg \to Q\bar{Q}q, \quad \bar{q}g \to Q\bar{Q}\bar{q} \tag{10}$$

The quarkonia produced from $O(\alpha_s^2)$ subprocess can have only small p_T, being of the order of the intrinsic transverse momentum of the incoming partons. On the other hand, the $O(\alpha_s^3)$ processes will yield large ($\sim O(\mathrm{GeV})$) p_T for the quarkonium with the light parton in the final state constituting a jet . Thus the $J/\psi(\Upsilon)$ produced at large-p_T in the SL model come from $2 \to 3$ subprocesses.

The matrix elements squared, appropriately averaged, for these processes have been computed. There are clearly two classes of diagrams—those involving one gluon, and those with three. We shall denote the squared matrix elements by A and B respectively. They depend on the momenta of all the five particles. Instead of reproducing the lengthy expressions for them, we refer the reader to the original work [32]. For computing p_T-distributions of the quarkonia we will need cross-sections more differential than the expression in eq. (8).

The phase-space for these processes is 6-dimensional. We consider the kinematics in the EHLQ [33] conventions, modified to account for massive Q and $\bar{Q}$. Defining the parton momenta in their center of mass, one sees that the three final state particles lie in a plane.

We choose this to be the xy-plane, and orient our axes by choosing the jet to be in the positive x-direction. The 4-momenta of the Q, $\bar{Q}$ and the jet are given, respectively, by

$$\begin{aligned} p_3 &= \frac{\sqrt{\hat{s}}}{2}\, x_3(1, \beta_3 \cos\theta_{35}, \beta_3 \sin\theta_{35}, 0), \\ p_4 &= \frac{\sqrt{\hat{s}}}{2}\, x_4(1, \beta_4 \cos\theta_{45}, \beta_4 \sin\theta_{45}, 0), \\ p_5 &= \frac{\sqrt{\hat{s}}}{2}\, x_5(1, 1, 0, 0), \end{aligned} \tag{11}$$

where $\beta_i = \sqrt{1 - 4M_Q^2/x_i^2 s}$ and the angles are given by

$$\cos\theta_{35} = \frac{(\beta_4 x_4)^2 - (\beta_3 x_3)^2 - x_5^2}{2\beta_3 x_3 x_5} \quad \text{and} \quad \cos\theta_{45} = \frac{(\beta_3 x_3)^2 - (\beta_4 x_4)^2 - x_5^2}{2\beta_4 x_4 x_5}. \tag{12}$$

Furthermore, energy-momentum conservation implies $x_3 + x_4 + x_5 = 2$, $(0 \le x_i \le 1)$, leaving only two independent variables in the equations above. In addition to x_1 and x_2 of eq. (8), two more variables are needed to specify the momenta of the incoming partons in this frame. Choosing these to be the Euler angles (θ, ϕ), we get

$$\begin{aligned} p_1 &= \frac{\sqrt{\hat{s}}}{2}\, (1, -\sin\theta\cos\phi, -\sin\theta\sin\phi, -\cos\theta), \\ p_2 &= \frac{\sqrt{\hat{s}}}{2}\, (1, \sin\theta\cos\phi, \sin\theta\sin\phi, \cos\theta). \end{aligned} \tag{13}$$

We can eliminate θ in favour of the transverse momentum of the pair (which is equal to that of the jet) through the relation

$$p_T = \frac{\sqrt{\hat{s}}}{2}\, x_5 \sqrt{\cos^2\theta + \sin^2\theta \sin^2\phi}. \tag{14}$$

Similiarly we can write the Feynman scaling variable x_F for J/ψ as

$$x_F = \frac{1}{2}\left[(x_1 + x_2)x_5 \sin\theta\cos\phi + (x_2 - x_1)(x_3 + x_4)\right]. \tag{15}$$

The E772 data has cuts on this x_F which we include in our computations.

Using the above kinematic relations the fully differential cross section for J/ψ-production computed to order α_s^3 can be written down as below:

$$\frac{d\sigma_{pA}}{dx_1 dx_2 dx_3 dx_4 d\phi dp_T} = \frac{\alpha_s^3 p_T}{16\pi s x_1 x_2 x_5^2 \cos\theta \cos^2\phi}$$
$$\Bigg[\frac{1}{9}\sum_q \Big\{f_{q/p}(x_1) f_{\bar{q}/A}(x_2) + f_{\bar{q}/p}(x_1) f_{q/A}(x_2)\Big\} A(p_3, p_4, -p_1, -p_2, p_5)$$
$$-\frac{1}{24}\sum_q \Big\{f_{g/p}(x_1) f_{q/A}(x_2) + f_{q/p}(x_1) f_{g/A}(x_2)\Big\} A(p_3, p_4, p_5, -p_1, -p_2) \qquad (16)$$
$$-\frac{1}{24}\sum_q \Big\{f_{g/p}(x_1) f_{\bar{q}/A}(x_2) + f_{\bar{q}/p}(x_1) f_{g/A}(x_2)\Big\} A(p_3, p_4, -p_1, p_5, -p_2)$$
$$+\frac{1}{64} f_{g/p}(x_1) f_{g/A}(x_2) B(p_4, p_3, p_5, -p_1, -p_2)\Bigg].$$

This is the cross section formula which together with appropriate structure functions, chosen from section II, we integrated over the kinematic region corresponding to the E772 experimental cuts [17,18] to compute the p_T distributions for the quarkonia J/ψ and Υ.

B. Colour Singlet Model

The colour singlet model was first developed for photoproduction of quarkonia [34] and later generalised to the hadronic production [23]. In this model one projects out the state with appropriate spin, parity and colour assignments from the full $Q\bar{Q}$ production amplitude to match the quantum numbers of the resonance under consideration. The projection is done at the level of hard scattering amplitude itself and this yields a multiplicative factor related to the quarkonium wave function at the origin in co-ordinate space. The effect of the hadronisation of the $Q\bar{Q}$ pair into the quarkonium is thus contained in this factor. For an S-wave resonance this multiplicative factor is the wave function, $R(0)^2$, at the origin whereas for a P-wave resonance it is the derivative of the wave function at the origin, $R_1'(0)^2$. $R(0)$ is related to the measured, leptonic $^3S_1$ width by

$$\Gamma_{\ell\bar{\ell}}(^3S_1) = \frac{4\alpha^2 e_Q^2 R(0)^2}{M^2} \qquad (17)$$

where α is the electromagnetic coupling, e_Q is the quark charge in units of proton charge and M is the mass of the quarkonium. $R_1'(0)$ can be related to the total hadronic width of the resonance by assuming it to be approximately the same as its gluonic width given by,

$$\Gamma_{gg}(^3P_0) = \frac{96\alpha_s^2 R_1'^2(0)}{M^2} \tag{18}$$

with α_s being the running strong coupling.

The model is known to give a good description of the kinematical distributions in leptoproduction [35] and hadroproduction [23,36] of J/ψ. However, there is a considerable uncertainty in the overall normalisation. Even after using the QCD corrected version of eq. (17) the data [35] required a K-factor of 2.4. This large K-factor is perhaps due to the nonrelativistic treatment of the quarkonium J/ψ in arriving at the hadronisation factor $R(0)^2$. Once again, for ratios of cross-sections at the same colliding energy, which we will consider here, the precise value of K-factor plays no role; we assume it to have no nuclear dependence.

The quarkonium production cross-section for the $^{2S+1}L_J$ quarkonium state in this model is given by

$$\begin{aligned}\sigma^{CS}(p+A \to\ ^{2S+1}L_J + X) = \sum_{p_1,p_2,p_3} \int_{p_T^{\min}}^{p_T^{\max}} dp_T \int_{y_1^{\min}}^{y_1^{\max}} dy_1 \int_{y_2^{\min}}^{y_2^{\max}} dy_2\ 2p_T x_1 x_2 \\ \times \left[f_{p_1/p}(x_1) f_{p_2/A}(x_2) + f_{p_2/p}(x_1) f_{p_1/A}(x_2)\right] \\ \times d\hat{\sigma}/d\hat{t}(p_1 + p_2 \to\ ^{2S+1}L_J + p_3)\end{aligned} \tag{19}$$

Here x_1, x_2 again denote the momentum fractions of the proton and nuclear target respectively carried by the partons p_1, p_2, $f_{p_i/h}$ are the parton density distribution functions and $d\hat{\sigma}/d\hat{t}$ denotes the differential subprocess cross-section. Here y_1, y_2 denote the rapidities of the quarkonium and the jet respectively and p_T is the transverse momentum of the quarkonium. The variables x_1, x_2 are given in terms of y_1, y_2 by

$$\begin{aligned} x_1 &= \frac{1}{2}\left[\bar{x}_T e^{y_1} + x_T e^{y_2}\right] \\ x_2 &= \frac{1}{2}\left[\bar{x}_T e^{-y_1} + x_T e^{-y_2}\right] \end{aligned} \tag{20}$$

In the above equation $x_T = \frac{2p_T}{\sqrt{s}}$, $\bar{x}_T = \sqrt{x_T^2 + 4\tau}$ with $\tau = M^2/s$. The total allowed range of integration over y_1, y_2, for a given value of p_T is given by

$$|y_1| \leq \cosh^{-1}\left(\frac{1+\tau}{\bar{x}_T}\right)$$

$$-\ell n\left(\frac{2-\bar{x}_T\exp(-y_1)}{x_T}\right) \leq y_2 \leq \ell n\left(\frac{2-\bar{x}_T\exp(y_1)}{x_T}\right) \tag{21}$$

$\hat{s}, \hat{t}, \hat{u}$ are the Mandelstam variables of the subprocess given by

$$\hat{s} = x_1 x_2 s; \quad \hat{t} = M^2 - x_1\sqrt{s(p_T^2+M^2)}e^{-y_1}; \quad \hat{u} = -x_1 p_T\sqrt{s}e^{-y_2}.$$

At the lowest order in the strong coupling, $O(\alpha_s^2)$, there is no parton p_3 in the final state; one has only the gluon fusion process

$$gg \rightarrow\ ^1S_0,\ ^3P_{0,2} \tag{22}$$

The quarkonium so produced has $p_T \simeq 0$. At $O(\alpha_s^3)$, the $gq(g\bar{q})$ and $q\bar{q}$ scatterings give rise to $^1S_0$, ^3P_J resonances (χ states) via

$$gq(\bar{q}) \rightarrow\ ^1S_0,\ ^3P_J + q(\bar{q});$$

$$q\bar{q} \rightarrow\ ^1S_0,\ ^3P_J + g \tag{23}$$

while the $^3S_1$ resonance can be produced directly as well via the gg subprocess,

$$gg \rightarrow\ ^1S_0,\ ^3S_1,\ ^3P_J + g \tag{24}$$

The ^3P_J states can decay into $^3S_1$ states via the radiative decay

$$^3P_J \rightarrow\ ^3S_1 + \gamma\ \ , \tag{25}$$

thus giving to rise to indirect contribution to the production of $^3S_1$ in addition to that of eq. (24). The expressions for the differential cross-section for the various subprocesses are available [23,37] and are not reproduced here.

Note that according to this model $^3P_1$ production is not possible at $O(\alpha_s^2)$ and hence the total $^3P_1$ rates are expected to be small compared to that of $^3P_0$,$^3P_2$. However this seems to be belied by the data [38] on hadroproduction of ^3P_J charmonium states. Since soft gluons, ignored as a part of the model ansatz, are likely to be more relevant in this case,

this possibly points to problems with the CS model for the $p_T \simeq 0$ quarkonium production. However, we use it here only for large-p_T ($\sim O$ (GeV)) quarkonium production where the soft gluons most likely do not play such a significant role.

We compute the ${}^3S_1$ $J/\psi(\Upsilon)$ production cross-section including both the direct contribution of eq. (24) and the contribution from the decay of ${}^3P_J$ states where ${}^3P_J$ state cross-sections are computed using eqs. (23) and (24). Since the Υ produced in process in eq. (25) carries very little energy, we assume the kinematical variables for the ${}^3P_J$ and ${}^3S_1$ resonance to have essentially the same values. The $d\sigma/dp_T$ is obtained using eq. (19). The E772 [17,18] cuts on the Feynman x_F of the resonance were implemented by restricting the y_1-integration between $y_1^{\min}$ and $y_1^{\max}$, which are related to the allowed range of x_F, $x_F^- < x_F < x_F^+$, by

$$y_1^{\min} = \ell n \left(\frac{x_F^-}{\bar{x}_T} + \sqrt{\left(\frac{x_F^-}{\bar{x}_T}\right)^2 + 1} \right)$$

$$y_1^{\max} = \ell n \left(\frac{x_F^+}{\bar{x}_T} + \sqrt{\left(\frac{x_F^+}{\bar{x}_T}\right)^2 + 1} \right) \quad . \tag{26}$$

Tables II and III give the details of the set of the resonance parameters which we used for our computations. The masses of all the resonances are taken from the latest compilation of particle properties [8]. Note here that the value of the $R(0)^2$ for the S–wave resonances ψ and ψ' are determined from the updated measurement of the letonic decay width [8] while the $R(0)^2$ for the Υ system and $R_1'(0)^2$ values for both the ψ and the Υ system have been taken from ref. [23].

C. Comparison of the Hadronisation Models

From the above discussion, it should be clear that the two hadronisation models differ quite significantly in the time scale for quarkonium formation. In the CS model it is the same as the perturbative time scale ($\sim 1/2M_Q \simeq 0.07$ fm for $Q = c$) whereas in the SLD case it is a typical hadronic scale ($\sim 1\ fm$). As a result, the only effect that a medium like

the Quark–Gluon–Plasma (QGP) can have in the first case will be on the propagation of the quarkonium, whereas in the SLD picture the formation process itself can be affected by the QGP environment.

The kinematics of the two models is also quite different. In the CS case basic hard subprocess which gets convoluted with the parton densities (as in eq. (19)) is a $2 \to 1$ subprocess for $O(\alpha_s^2)$ case and $2 \to 2$ subprocess for $O(\alpha_s^2)$ case of large-p_T quarkonium production. In the SLD case, these are respectively a $2 \to 2$ subprocess and a $2 \to 3$ subprocess. Hence, in principle the momentum division between the large-p_T quarkonium and the light parton jet can be quite different in the two cases and it is worthwhile to find out whether perhaps the p_T distribution $d\sigma/dp_T$ for quarkonium could help discriminate between these two models of hadronisation.

D. Gluon dominance

In Ref. [9] it was argued that the E772-data are described by $O(\alpha_s^2)$ partonic cross-section and further that this $O(\alpha_s^2)$ production cross-section of eq. (8), is dominated by the $gg \to Q\bar{Q}$ contribution of eq. (9). Then the ratio of experimentally measured cross-sections for different targets, at a given value of x_F and τ directly yields the ratio of gluon densities for the two targets at an x_2 given by

$$x_{1,2} = \frac{1}{2}\left(x_F \pm \sqrt{x_F^2 + \tau^2}\right) \quad . \tag{27}$$

It is worth noting that only for the case of $2 \to 1$ kinematics the x_F of the quarkonium is related to x_1 and x_2 through the oft-used simple relation of eq. (27). As can be seen from eq. (15), this is no longer true for quarkonium production at large-p_T via the $2 \to 3$ subprocess of SLD or also the $2 \to 2$ subprocess in CS-model. Considering the rather large p_T-range of the E772-data (≤ 2.25 GeV for the J/ψ and ≤ 4 GeV for the Υ), it seems to be an oversimplification to employ either the eq. (27) or indeed the $O(\alpha_s^2)$ subprocess itself (unless one tolerates rather large values of intrinsic k_T for the partons) . As mentioned

above, since the CS-model is perhaps unreliable for $p_T \sim 0$, even if eq. (27) were to be valid one still further needs the assumption of gluon dominance if the SLD-model of hadronisation is employed.

In support of their argument of gluon dominance Ref. [9] considered the ratio of parton luminosities,

$$R_{qg} = \frac{F_{qq}}{F_{gg}} = \frac{\sum_{q=u,d,s} \left(f_{q/h}(x_1) f_{\bar{q}/h}(x_2) + f_{\bar{q}/h}(x_1) f_{q/h}(x_2) \right)}{f_{g/h}(x_1) f_{g/h}(x_2)} \tag{28}$$

for a particular parametrisation of the parton densities in the proton viz. DFLM [39] and showed it to be rather small in the x_F-range of interest (using eq. (27)). It turns out, however, that this demonstration of gluon-dominance strongly depends on the choice of parton densities used. We plot in Fig.2 the ratio in eq. (28) as a function of x_F for $\sqrt{\tau} = 0.0775$ corresponding to the nucleon-nucleon c.m. energy of the E772 experiment and $M_{Q\bar{Q}} = M_{J/\psi}$. x_1 and x_2 for a given value of x_F are obtained from eq. (27). The different curves of Fig.2 correspond to various popular choices of the parton densities: the older parametrisations DFLM [39], DO1, DO2 [40] and GHR [41], and the newer MT1, MT2, MT3 [42] and ON [43]. For the DFLM parametrisation which the authors of Ref. [9] use the approximation of gluon dominance is indeed good for low values of x_F ($x_F \lesssim 0.3$) . However, E772 data goes upto $x_F \simeq 0.65$. Moreover, we also see from Fig.2 that gluon dominance crucially depends on the choice of parton density parametrisation in a proton. For the MT parametrisation, e.g., the $q\bar{q}$ contribution is $\sim 60\%$ of the gg contribution at the largest x_F value considered ($x_F = 0.5$). As Fig.3 shows the situation becomes much worse for Υ with $\sqrt{\tau} = M_\Upsilon/\sqrt{s} = 0.2365$. Thus it is clear that the extraction of $\rho_g(x)$ by using gluon dominance and then simply taking the ratio of experimentally measured J/ψ-cross sections for the nuclear and the nucleon target has an intrinsic uncertainty of $\sim$ 10-15 %. In view of the fact that the expected deviation of ρ_g from unity, viz. the EMC effect, is also of the same order of magnitude, we feel that this is not a very effective or precise determination of ρ_g.

The models for EMC effect always give a parametrisation for nuclear parton densities for a specific parametrisation of parton densities in proton. In all the models we use, the

choice of reference parton densities in the proton is different from all the above mentioned parametrisations. We have checked that our observation about lack of the gluon dominance holds for these parametrisations as well.

In view of the above discussion, attempts to extract the nuclear gluon density from the high statistics E772 data appear to have both conceptual problems and sizeable theoretical uncertainties. An alternative, albeit a less ambitious, approach may be to check the consistency between the predicted ratios of differential cross-sections $d\sigma/dp_T$ for various models of nuclear parton densities and the high statistics E772 data. One may thus hope to pin them down or even expose their deficiencies using the high quality and more differential data. Since the small-p_T region is plagued by the issues of intrinsic transverse momentum of the inital partons or resummations of higher order diagrams, we choose to investigate only the large-p_T E772 data and compute only the $O(\alpha_s^3)$ contributions to the cross-sections. This compels us to ignore the data on p_T-integrated x_F distributions or their ratios since they should receive substantial contribution from the small-p_T region. In order to test the x_F-dependence of our pQCD calculations, it would be desirable to have the data integrated in different, at least two, ranges of p_T.

E. Results

The E772 experiment has provided data for the ratio

$$R^{J/\psi}(p_T) = \frac{d\sigma(pA \to J/\psi X)}{dp_T} \Big/ A\frac{d\sigma(pp \to J/\psi X)}{dp_T} \tag{29}$$

with an x_F-cut of $0.15 \leq x_F \leq 0.65$ on the J/ψ's, while for the Υ-production cross sections, they chose to present only $\alpha(p_T)$, where

$$\frac{d\sigma(pA \to \Upsilon X)}{dp_T} = A^{\alpha(p_T)}\frac{d\sigma(pp \to \Upsilon X)}{dp_T} \tag{30}$$

with a corresponding x_F-cut for Υ of $-0.2 \leq x_F \leq 0.6$. The nuclei used were carbon, calcium, iron and tungsten. Incorporating these x_F-cuts, using eqs. (15) and (26), we computed each of the individual p_T-distribution in eqs. (29-30) for both the SLD-model and the

CS-model and the three models of nuclear structure functions discussed in sect. II. Fig. 4 exhibits our results for the SLD-model for all the four nuclei along with the corresponding data from the E772 collaboration. The errors for theoretical predictions are purely statistical, arising from the Monte Carlo integration of the differential cross sections. One sees that for the lighter nuclei both the two-component models, namely, the gas model and the six-quark cluster model, describe the data well, especially if one takes into account a possible systematic error of a few per cent due to variations in input parameters such as M_c, Λ_{QCD} etc. For the tungsten nucleus, however, *none* of the models seems to to be in agreement with data. One could compare the CS–model results with the E772–data in a similar manner as well. Instead we choose to compare the results of the two hadronisation models directly since the theoretical results have a better precision. Fig. 5 shows the ratio of $R^{J/\psi}(p_T)$ for the SLD-model and the CS-model for each model of the nuclear parton densities, nucleus and p_T. The ratio of the ratios seems to lie in almost all the cases within $\sim 5\%$ of unity. Considering the different kinematics of the two models and also the different physics of the quarkonium formation the agreement is really remarkable and it shows the robustness of the pQCD predictions. Note that even in the case of Tungsten both the models agree with each other rather well and thus have essentially the same discrepancy with the E772 data. Of course, the discrepancy in the case of tungsten does expose the inadequacy of all the three models of the EMC effect and the corresponding parametrisation of the nuclear parton densities considered here but the generalagreement in other cases, on the other hand suggests that the structure function effects indeed do describe the bulk of the p_T-data. One may note here that the lowest p_T value at which we performed these computations is somewhat low, being 0.79 GeV. Presumably, the anticipated large QCD-corrections at such low p_T affect all the cross sections similarly and thus cancel out in the ratio, resulting in a good description of the data. A remark on the gluon dominance may be in order as well. Extracting the contribution for individual parton subprocesses, we typically found the dominant contribution to be from gg and qg processes which were in the range of 75-80% and 25-20% respectively. Thus, the quark contributions are sizeable and an independent determination

of the gluon density from these data are not possible without making an ansatz for the quark distributions.

Fig. 6 shows a comparison of our calculations for the SLD-model for Υ-production with the E772-data. At each p_T in the range of 1-4 GeV, the calculations for each individual $d\sigma/dp_T$ were done as for J/ψ-production by incorporating the experimental x_F-cut. The results for differential cross sections were then fitted as a power law in A to obtain $\alpha(p_T)$. One sees a similar general agreement for the gas model and the six-quark cluster model as for J/ψ-production at moderate values of p_T. At the largest p_T, however, the E772-data rise too sharply compared to any model and could possibly indicate that these models tuned to earlier large x-data have to be better tuned to perform well in the small x-region. Fig. 7 shows that this disagreement at large p_T, as well as the agreement at lower p_T, are once again features which do not depend on the hadronisation model. The figure shows the ratio of the results obtained for the SLD-model and the CS-model for the experimental cuts of E772 as a function of p_T and they are within $\sim 5\%$ of each other. Thus within the framework of pQCD these data too are explicable in terms of changes of nuclear structure functions. As one can expect, the contribution of the qg subprocess in the case of Υ–production is even larger, being typically $\sim$40% in comparison to that of the gg subprocess which almost accounted for the rest.

IV. DIMUON PRODUCTION

The $J/\psi(\Upsilon)$ is detected most efficiently via its decay into a $\mu^+\mu^-$ pair. Hence any critical evaluation of J/ψ suppression as a signal of QGP formation also needs a good understanding of the p_T- and A-dependence of this continuum $\mu^+\mu^-$ background. An experimental measurement of the A-dependence of the dimuon pair production can also provide an independent probe of the nuclear parton densities and an evidence in favour of the universality of the EMC-effect, *i.e.*, its process independence. In fact, one of the earliest theoretical attempts to understand the dimuon data had postulated [44] A-dependent sea density even

before the EMC effect was experimentally discovered. The production of massive $\mu^+\mu^-$ pairs (DY) in hadronic collisions is now well understood in the framework of pQCD [22]. The dimuon production at small p_T and large x_F is essentially well described in terms of $q\bar{q}$ annihilation process in spite of the large higher order corrections. For large p_T of the $\mu^+\mu^-$ pair the production cross-section is given by the $O(\alpha_s)$ subprocesses involving gluons viz.,

$$q + g \to \gamma^* + q \to \mu^+\mu^- + q; \quad q + \bar{q} \to \gamma^* + g \to \mu^+\mu^- + g \tag{31}$$

The high statistics E772-experiment [19] has provided data for nuclear-dependence of proton-induced pair production over a wide range of x_F and p_T values. The data on the ratio of the *integrated* dimuon yield for different nuclei were compared with theoretical predictions, obtained by using the $q\bar{q}$ annihilation process, for various models of the EMC effect. It seemed [19] to rule out the 6-quark cluster model [27]. However, a later comparison [11] with an improved version of the model, described in sect. II.C, showed that this model too can be consistent with the information on the ratio of the integrated dimuon yields. The E772 experiment [19] has also presented p_T distributions (integrated over x_F and $M^2_{\mu^+\mu^-}$) and x_F distributions (integrated over p_T and $M^2_{\mu^+\mu^-}$) for the dimuon pairs. A comparison of ratios of these differential distributions for different targets with the predictions of various models of EMC effect can discriminate between them more effectively. Since the $O(\alpha_s)$ pQCD calculation is valid only at large-p_T, we restrict ourselves to the p_T distributions. The x_F distributions are integrated over the complete range of p_T and hence dominated by $p_T \sim 0$ data, which once again forced us to ignore them in this leading order pQCD analysis.

The kinematics of the DY $\mu^+\mu^-$ pair production at large p_T in the $O(\alpha_s)$ subprocesses of eq. (31) is very similar to the kinematics of the $J/\psi(\Upsilon)$ production in the colour-singlet model, discussed in sect. III.B. Its differential cross-section is given by

$$\frac{d\sigma}{dM^2_{\mu^+\mu^-}dp_T^2} = \int_{y_1^{\min}}^{y_1^{\max}} dy_1 \int_{y_2^{\min}}^{y_2^{\max}} dy_2 \; x_1 x_2 \Big\{ P_{qg} \; \frac{d\hat{\sigma}(qg \to \mu^+\mu^- q)}{dM^2_{\mu^+\mu^-}d\hat{t}} + P_{q\bar{q}} \; \frac{d\hat{\sigma}}{dM^2_{\mu^+\mu^-}d\hat{t}} \; (q\bar{q} \to \mu^+\mu^- g) \Big\} \;\; , \tag{32}$$

where

$$P_{qg} = \sum_{q,\bar{q}} \Big[f_{q/p}(x_1) f_{g/A}(x_2) + f_{g/p}(x_1) f_{q/A}(x_2) \Big]$$

$$P_{q\bar{q}} = \sum_{q} \Big[f_{q/p}(x_1) f_{\bar{q}/A}(y_2) + f_{\bar{q}/p}(x_1) f_{q/A}(x_2) \Big] \quad , \tag{33}$$

with

$$\frac{d\hat{\sigma}}{d\hat{t}} \, (qg \to \mu^+\mu^- q) = \frac{\alpha_s \alpha_{em}^2 e_q^2}{9 M^2_{\mu^+\mu^-}} \cdot \frac{\left\{ \left(\hat{s} - M^2_{\mu^+\mu^-} \right)^2 + \left(u - M^2_{\mu^+\mu^-} \right)^2 \right\}}{-\hat{s}^3 \hat{u}}$$

$$\frac{d\hat{\sigma}}{d\hat{t}} \, (q\bar{q} \to \mu^+\mu^- g) = \frac{8 \; e_q^2 \alpha_s \alpha_{em}^2}{27 \; M^2_{\mu^+\mu^-}} \; \frac{\left\{ \left(\hat{t} - M^2_{\mu^+\mu^-} \right)^2 + \left(\hat{u} - M^2_{\mu^+\mu^-} \right)^2 \right\}}{\hat{s}^2 \hat{t} \hat{u}} \quad . \tag{34}$$

Here y_1, y_2 are the rapidities at the $\mu^+\mu^-$ pair and the associated jet respectively. The Mandestam variables $\hat{s}$, $\hat{t}$ and $\hat{u}$, the relation of the momentum fractions x_1 and x_2 in terms of y_1, y_2, the integration limits and their relation with the experimental x_F-cut ($x_F > 0$) are precisely the same as those given in sect. III.B for the colour singlet model with M^2 replaced in all the formulae by $M^2_{\mu^+\mu^-}$. We will therefore not repeat them here.

Experimental information [19] is available for the ratio

$$R^{DY} = \frac{d\sigma^{DY}}{dp_T} \, (pA \to \mu^+\mu^- X) \Big/ \frac{d\sigma^{DY}}{dp_T} \, (pp \to \mu^+\mu^- X) \tag{35}$$

where $d\sigma^{DY}/dp_T$ is the differential DY cross section integrated over the continuum region (avoiding the resonances) $4 < M_{\mu^+\mu^-} < 9$ GeV and $M_{\mu^+\mu^-} \geq 11$ GeV, with $x_F > 0$.

Integrating eq. (32) over the above experimental cut of $x_F > 0$ and $4 < M_{\mu^+\mu^-} < 9$ as well as $M_{\mu^+\mu^-} > 11$ GeV, we compute the ratio R^{DY} of eq. (35) for all the different nuclear targets used in the experiment for each of the three sets of nuclear and nucleon parton densities described before. $M^2_{\mu^+\mu^-}$ was used as the scale for α_s in eqs. (34).

Fig. 8 exhibits the results of our computation for the four different nuclei with the corresponding data. Again we see similar to the case of resonance production that the general trends of the data are well described by the model predicltions for the gas model and the 6-quark cluster model.

V. CONCLUSION

In conclusion, we have shown in this paper that the high statistics data E772 on the nuclear dependence of the production of quarkonia (J/Ψ and Υ) *and* dimuon pairs at large p_T can be entirely explained in terms of the same nuclear structure functions, in the frameowrk of pQCD. All our theoretical calculations contained no arbitrary free parameters; only existing models of the EMC-effect with their already fixed values of parameters were used. We employed two popular models of hadronization of the $Q\bar{Q}$-pair into the quarkonia. In spite of their big kinematical differences, we found both to yield predictions which were within $\sim 5\%$ of each other. This shows the robustness of the pQCD approach and underlines the importance of the nuclear structure function effects in understanding the behaviour of these data. Similar conclusions [6,7] about the independence of hadronization mechanism and the universality of the nuclear structure functions in various hard scattering processes [3] have been obtained before but the accuracy of the present data makes them now much stronger. Recently it was argued [45] that quantum mechanical coherence and interference effects destroy factorisation in quarkonia production and hence prevent the possibility of using the same nuclear structure functions for different final states. However, the consistency of both the quarkonia and the dimuon data with our calculations, points towards the correctness of ideas of universality of the structure functions, at least in the kinematic region probed in our analysis.

Our analysis also indicates that the accuracy of the data has now reached a stage so as to distinguish between various models of the EMC effect and the nuclear structure function parametrisations therein. Indeed, the inability of *all* models to make a better prediction for the tungsten nucleus than shown in Fig. 4, and the disagreement at the largest p_T value in Fig. 6, are hints for inventing better parametrizations of the nuclear dependence of the quark (and gluon) distributions. We also argued that the twin assumptions of gluon dominance and adequacy of the lowest order partonic cross section are unreliable due to the large x_F and p_T ranges of the E772-data. Extraction of the nuclear gluon density using them is likely

to be dominated by uncertainties as large as the gluonic EMC-effect itself.

We have examined here data at a fixed value of p_T but which have been integrated over the entire x_F region corresponding to the acceptance of the experiment. The integrated data are dominated by the data at small x_F values (or not-so-small x_2 values). Hence our non-inclusion of any shadowing effects for the nuclear parton densities can be justified. If one wants to critically use these data to study the shadowing effects in the nuclear parton densities, then it would be necessary to look at the nuclear effects in the p_T integrated data at large values of x_F (which will probe small values of x_2). The data on x_F distributions available currently is integrated over the entire range of p_T whereas our pQCD analysis is valid only for $p_T \geq 1$ GeV. If information about the x_F distributions integrated over only the large p_T region becomes available, it will help unravel the issue of nulear dependence of the J/Ψ, Υ and the dimuon production further.

REFERENCES

[1] EMC Collaboration, J.J. Aubert et al., Phys. Lett **B 123**, 275 (1983).

[2] For a review of the data on and models of the EMC effect see, e.g.; M. Arneodo, Nuclear Effects in Structure Functions, CERN-PPE/92-113.

[3] R.M. Godbole, in: Frontiers in particle physics, ed. Z. Ajduk, S. Pokorski and A.K. Wrobdewski (World Scientific, Singapore, 1990) p.483.

[4] R.M. Godbole and S. Gupta, Phys. Lett. **B 278**, 129 (1989).

[5] S. Gupta and Sridhar K., Phys. Lett. **B 197**, 259 (1987); Sridhar K., Z. Phys. **C55**, 401 (1992) .

[6] R.V. Gavai and S. Gupta, Z. Phys. **C49**, 663 (1991).

[7] R.M. Godbole and Sridhar K., Z. Phys. **C51**, 417 (1991).

[8] Review of Particle Particles, Phys. Rev. **D 45** (1992).

[9] S. Gupta and H. Satz, Z. Phys. **C55**, 391 (1992).

[10] L.N. Epele, C.A. Garcia Canal and M.B. Gay Ducati, Phys. Lett. **B 226**, 169 (1989).

[11] K.F. Lassila, U.P. Sukhatme, A. Harindranath and J. Vary, Phys. Rev. **C44**, 1188 (1991) .

[12] R.V. Gavai, R.M. Godbole and Sridhar K., Phys. Lett. **B 299**, 157 (1993).

[13] T. Matsui and H. Satz, Phys. Lett. **B 178**, 416 (1986).

[14] F. Karsch and R. Petronzio, Phys. Lett. B 193, 105 (1987) ; J. Blaziot and J.Y. Ollitrault, Phys. Lett. **B 199**, 199 (1987); M.-C. Chu and T. Matsui, Phys. Rev. **D37**, 1851 (1988); F. Karsch and R. Petronzio, Z. Phys. **C37**, 627 (1988).

[15] NA38 Collaboration, C. Baglin et al., Phys. Lett. **B220**, 471 (1989); *ibid*, **B255**, 459 (1991); *ibid*, **B251**, 460 (1990).

[16] R.V. Gavai and S. Gupta and Sridhar K., Phys. Lett. **B227**, 161 (1989); Nucl. Phys. **A498**, 483c (1989).

[17] D.M. Alde et al., Phys. Rev. Lett. **66**, 133 (1991).

[18] D.M. Alde et al., Phys. Rev. Lett. **66**, 2285 (1991).

[19] D.M. Alde et al., Phys. Rev. Lett. **64**, 2479 (1990).

[20] B.L. Combridge, Nucl. Phys. **B151**, 429 (1979).

[21] Z. Kunszt and E. Pietarinen, Nucl. Phys. **B164**, 45 (1980); R.K. Ellis and J.C. Sexton, Nucl. Phys. B282, 642 (1987).

[22] See, e.g., Applications of Perturbative QCD, R. D. Field, (Addison-Wesley, Redwood City, USA).

[23] R. Baier and R. Rückl, Z. Phys. **C19**, 251 (1983).

[24] M. Glück and E. Reya, Phys. Lett. **79B**, 453 (1978).

[25] S. Gupta and K. V. L. Sarma, Z. Phys. **C29**, 329 (1985).

[26] F.E. Close, R.G. Roberts and G.G. Ross, Phys. Lett. **B129**, 346 (1993).

[27] K.E. Lassila and U.P. Sukhatme, Phys. Lett. **B209**, 343 (1988); U.P. Sukhatme, G. Willk and K.E. Lassila, Z. Phys. **C53**, 439 (1992).

[28] CDHS Collaboration, J. G. H. de Groot et al., Z. Phys. **C17**, 283 (1983).

[29] S. Gupta, S. Banerjee and R.M. Godbole, Z. Phys. **C28**, 483 (1985).

[30] S. Gupta, Pramana **24**, 443 (1985).

[31] M. Sato, S. Coon, H. Pirner and J. Vary, Phys. Rev. **C33**, 1062 (1986).

[32] Second reference from Ref. [21].

[33] E. Eichten, I. Hinchliffe, K. Lane and C. Quigg, Rev. Mod. Phys. **56**, 579 (1984).

[34] E.L. Berger and D. Jones, Phys. Rev. D **23**, 1521 (1981).

[35] D. Allasia et al., Phys. Lett. **B258**,493 (1991); P. Amaudruz et al., Nucl. Phys. **B371**, 553 (1992).

[36] C. Albajar et al., Phys. Lett. **B273**, 540 (1991).

[37] R. Gastmans, W. Troost and T.T. Wu, Phys. Lett. **B184**, 257 (1989).

[38] E705 Collaboration, L. Antoniazzi, Phys. Rev. Lett. **70**, 383 (1993); Phys. Rev, **D46**, 4828 (1992).

[39] M. Diemoz, E. Ferroni, E. Longo and G. Martinelli, Z. Phys. **C39**, 27 (1988).

[40] D.W. Duke and J.F. Owens, Phys. Rev. **D30**, 49 (1984).

[41] M. Glück, E. Hoffman and E. Reya, Z. Phys. **C13**, 1 (1982).

[42] J. G. Morfin and Wu-Ki Tung, Z. Phys. **C52**, 13 (1991)

[43] J.F. Owens, Phys. Lett. **B 266**, 126 (1991).

[44] R.M. Godbole and K.V.L. Sarma, Phys. Rev. **D25**, 120 (1982).

[45] D. Kharzeev and H. Satz, CERN preprint, CERN-TH.7115/93.

TABLES

TABLE I. Model parameters for nuclei used in E772 experiment for gas model(T,ω) and six quark cluster model(ϵ).

A	T (MeV)	ω	ϵ
12	54	0.069	0.112
40	47	0.057	0.170
56	45	0.117	0.186
184	42	0.132	0.230

TABLE II. Resonance parameters used for $\psi, \psi^{'}$ and $\Upsilon, \Upsilon^{'}$.

Resonance R	M(MeV)	$R(0)^2(GeV)^3$	BF($R \rightarrow$ $^3S_1+$ neutrals)
ψ	3096	0.542	1.00
$\psi^{'}$	3686	0.307	0.55
Υ	9460	4.54	1.00
$\Upsilon^{'}$	10020	2.54	0.19

TABLE III. Resonance parameters used for χ^c and χ^b states.

Resonance R	M(MeV)	$R_1^{'}(0)^2/M^2(GeV)^3$	BF($R \rightarrow^3 S_1+$ neutrals)
χ_0^c	3415	9.1×10^{-3}	6.6×10^{-3}
χ_1^c	3510	9.1×10^{-3}	0.273
χ_2^c	3555	9.1×10^{-3}	0.135
χ_0^b	9860	1.5×10^{-2}	0.040
χ_1^b	9890	1.5×10^{-2}	0.290
χ_2^b	9915	1.5×10^{-2}	0.220

FIGURES

FIG. 1. Predictions for the ratio of the nuclear and nucleonic gluon density, ρ_g, of the three models of the EMC effect described in the text.

FIG. 2. The ratio $R_{qg} = \frac{F_{qg}}{F_{gg}}$ of Eq. (28) corresponding to J/ψ production at the FNAL energies for MT1(solid), MT2(long–dashed), MT3(medium–dashed), ON(short–dashed), GGR(dotted), GHR(dot–dashed), DO1(dot–dot–dashed) and DO2(inverted triangle) parametrisation of the parton densities.

FIG. 3. Same as in Fig. 2 but for Upsilon production at the FNAL energies.

FIG. 4. E772 data on the ratio $R^{J/\psi}$ of Eq. 29 compared with the predictions for the gas model(squares), six-quark cluster model(circles) and the rescaling model(open circles) of the EMC effect, obtained using the SLD for hadronisation.

FIG. 5. Ratio of the predictions for $R^{J/\psi}$ for the SLD and CS model of hadronisation, for the different nuclear parton densities. Notation is same as in Fig. 4.

FIG. 6. E772 data on $\alpha(p_T)$ of Eq. 30 compared with predictions of the three different models of the EMC effect mentioned in the text, using the SLD model of hadronisation. Notation is same as in Fig. 4.

FIG. 7. Ratio of $\alpha(p_T)$ predicted in the SLD and CS models of hadronisation for the three models of the EMC effect. Notation is the same as in Fig. 4.

FIG. 8. E772 data on the ratio R^{DY} of eq.35 compared with predictions of the three models of the EMC effect. Notation is same as in Fig. 4.

This figure "fig1-1.png" is available in "png" format from:

http://arxiv.org/ps/hep-ph/9402345v1

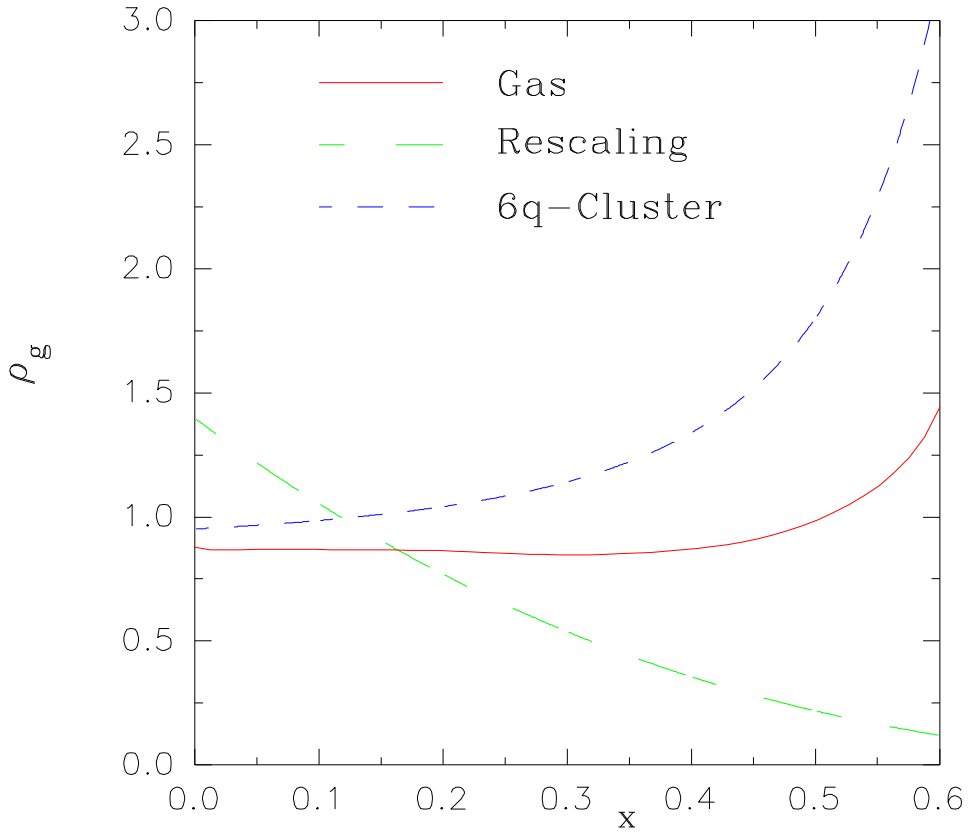
3.0
2.5
2.0
1.5
1.0
0.5
0.0
ρ_g
Gas
Rescaling
6q−Cluster
0.0
0.1
0.2
0.3
0.4
0.5
0.6
x

Figure 1

This figure "fig2-1.png" is available in "png" format from:

http://arxiv.org/ps/hep-ph/9402345v1

This figure "fig1-2.png" is available in "png" format from:

http://arxiv.org/ps/hep-ph/9402345v1

This figure "fig2-2.png" is available in "png" format from:

http://arxiv.org/ps/hep-ph/9402345v1

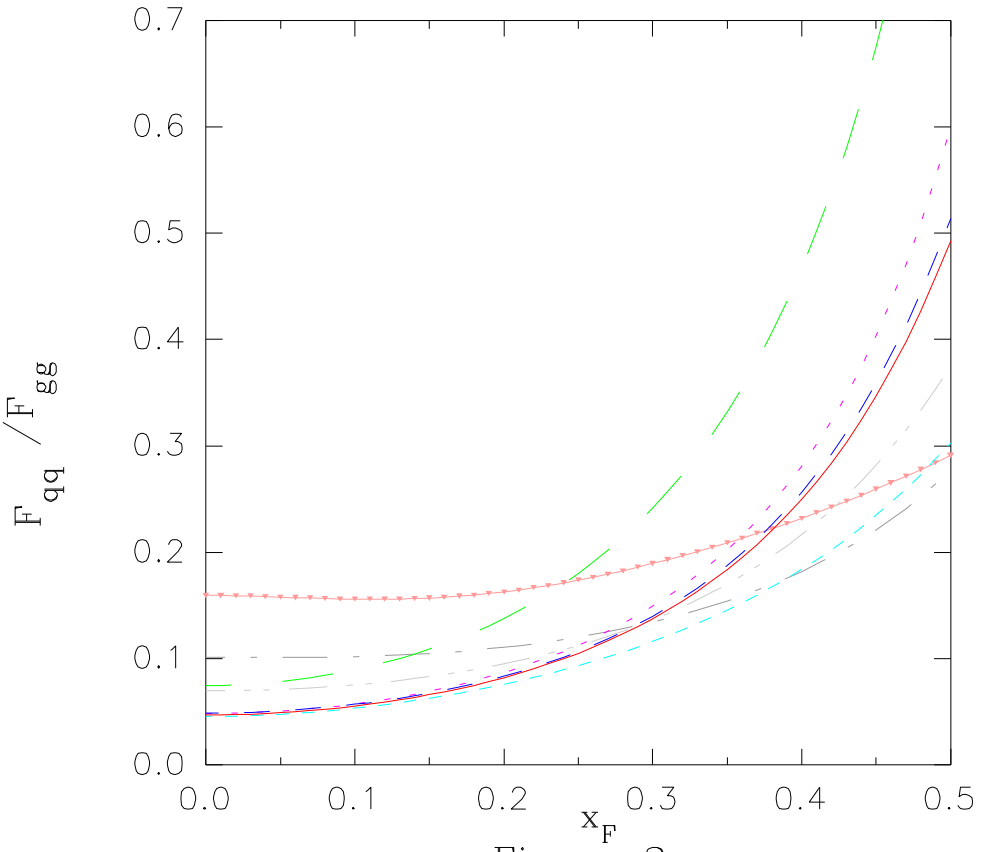

Figure 2

This figure "fig1-3.png" is available in "png" format from:

http://arxiv.org/ps/hep-ph/9402345v1

This figure "fig2-3.png" is available in "png" format from:

http://arxiv.org/ps/hep-ph/9402345v1

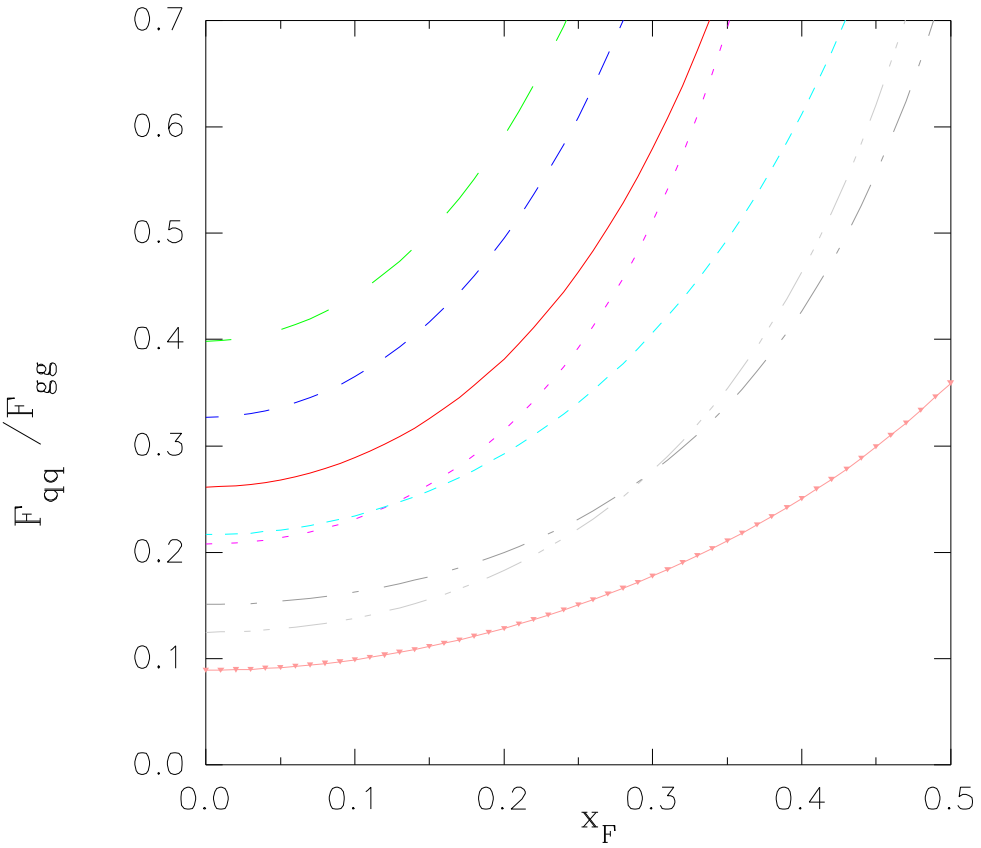

Figure 3

This figure "fig1-4.png" is available in "png" format from:

http://arxiv.org/ps/hep-ph/9402345v1

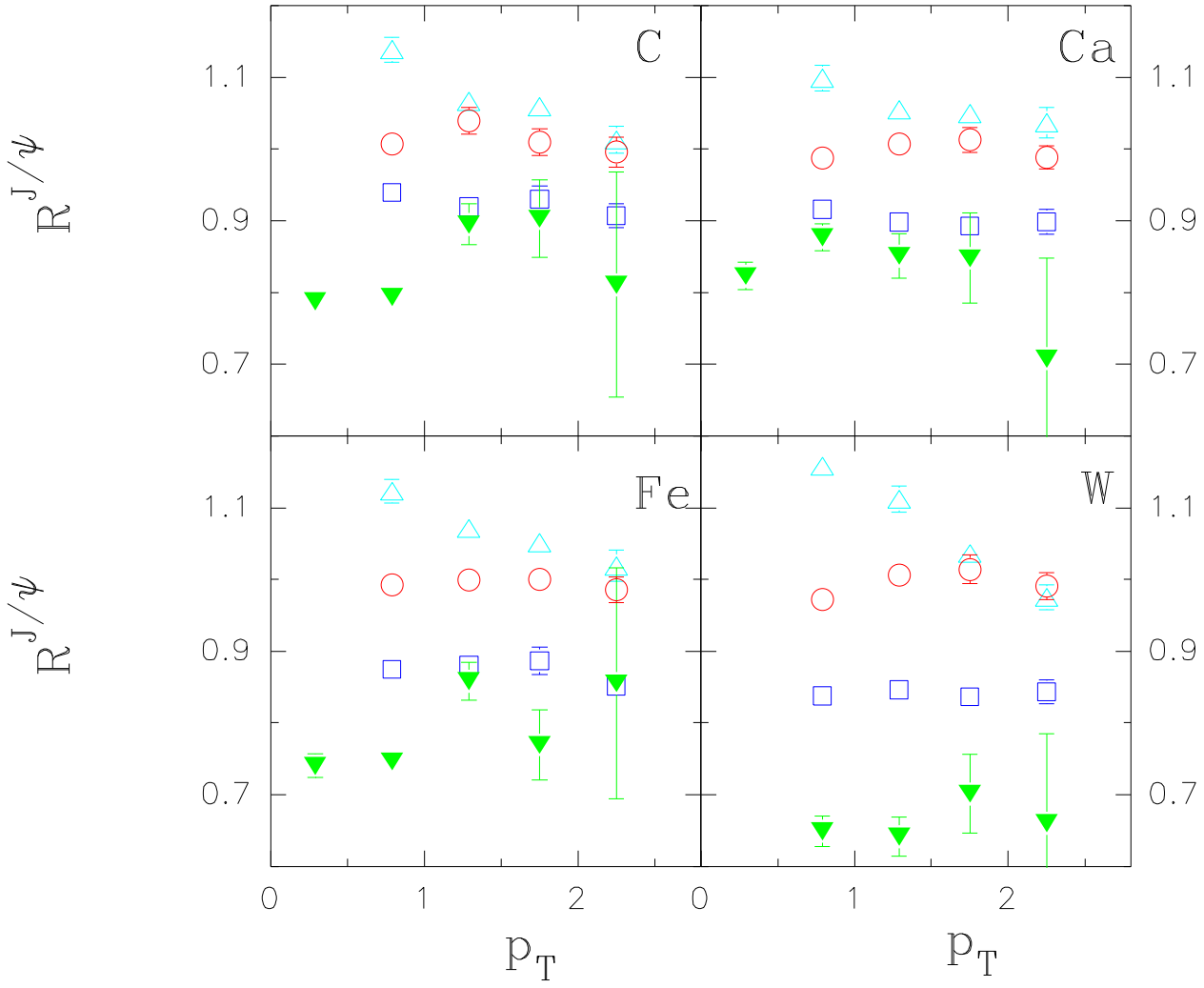

Figure 4

This figure "fig1-5.png" is available in "png" format from:

http://arxiv.org/ps/hep-ph/9402345v1

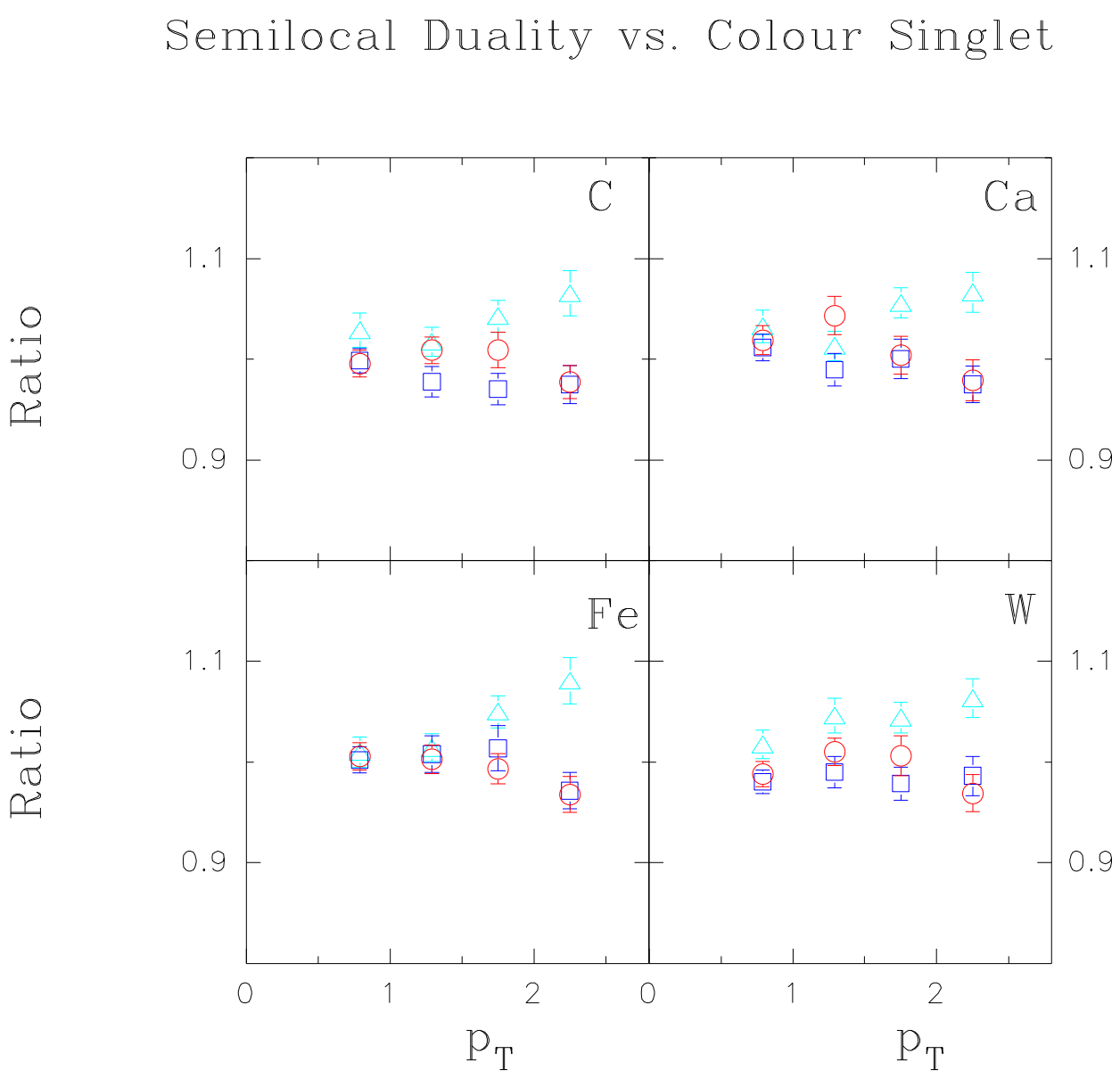
Semilocal Duality vs. Colour Singlet
C
Ca
Fe
W
Ratio
Ratio
1.1
0.9
1.1
0.9
1.1
0.9
1.1
0.9
0
1
2
0
1
2
p_T
p_T

Figure 5

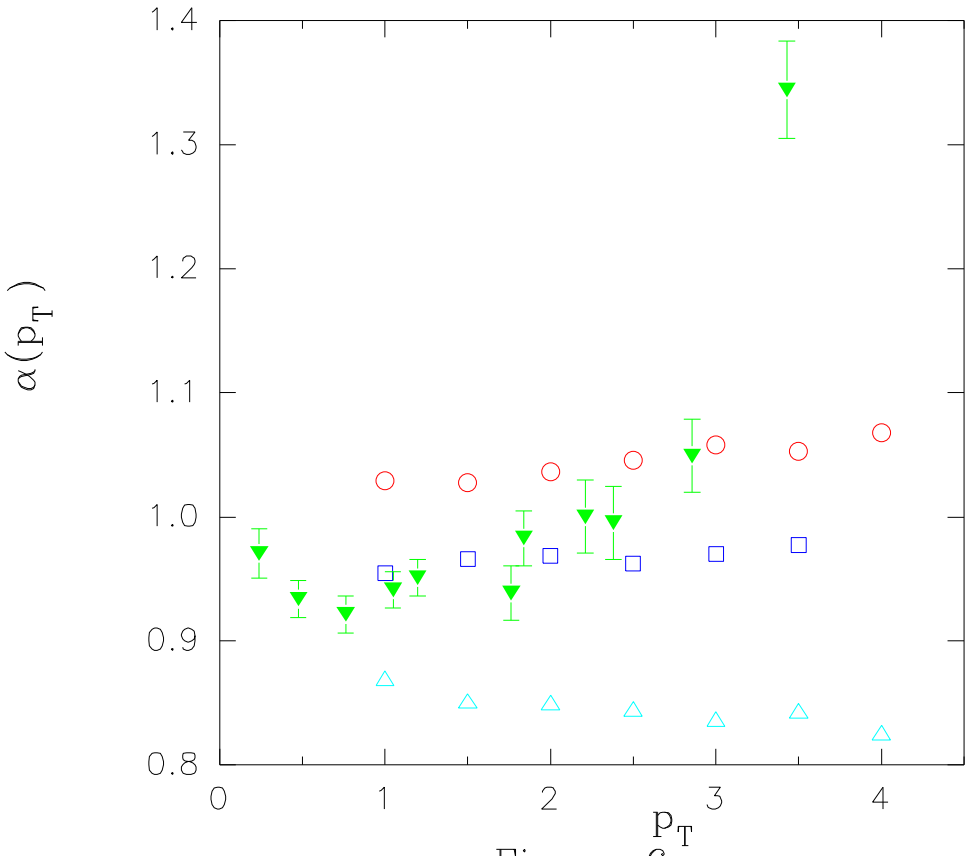

Figure 6

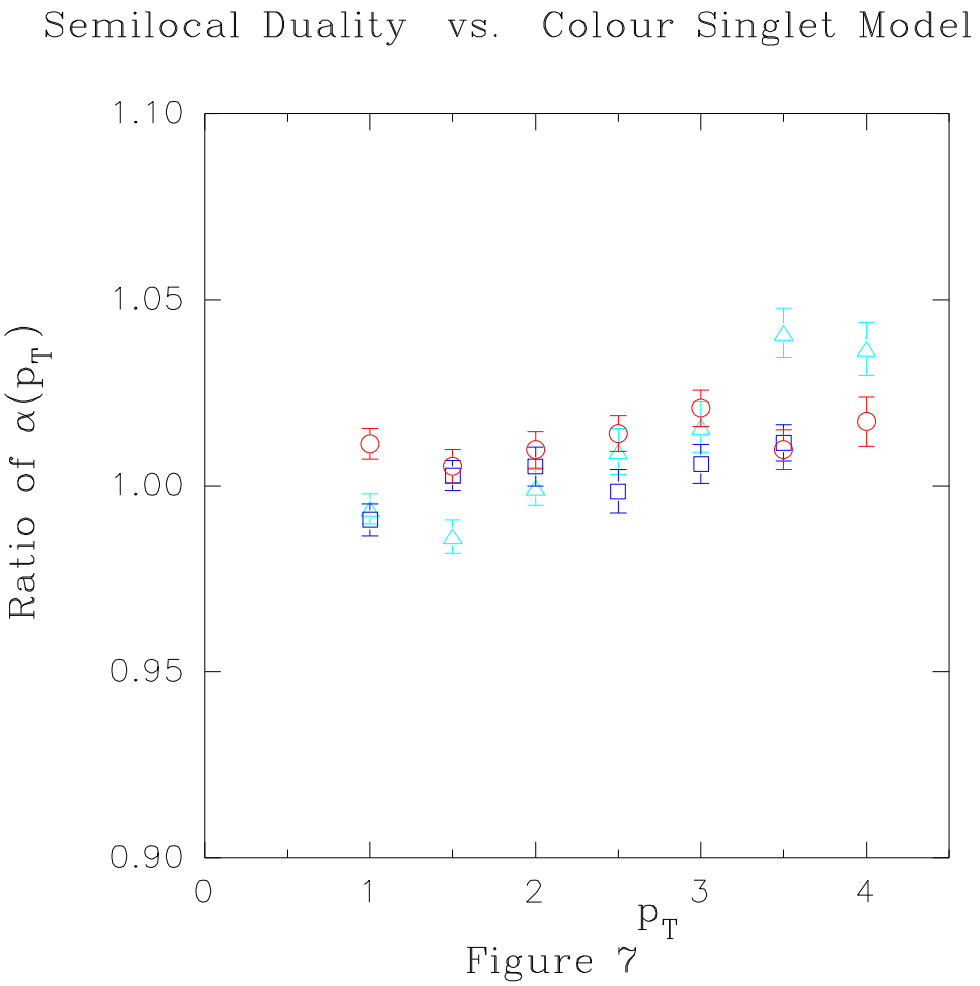
Semilocal Duality vs. Colour Singlet Model
Ratio of $\alpha(p_T)$
1.10
1.05
1.00
0.95
0.90
0
1
2
3
4
p_T

Figure 7

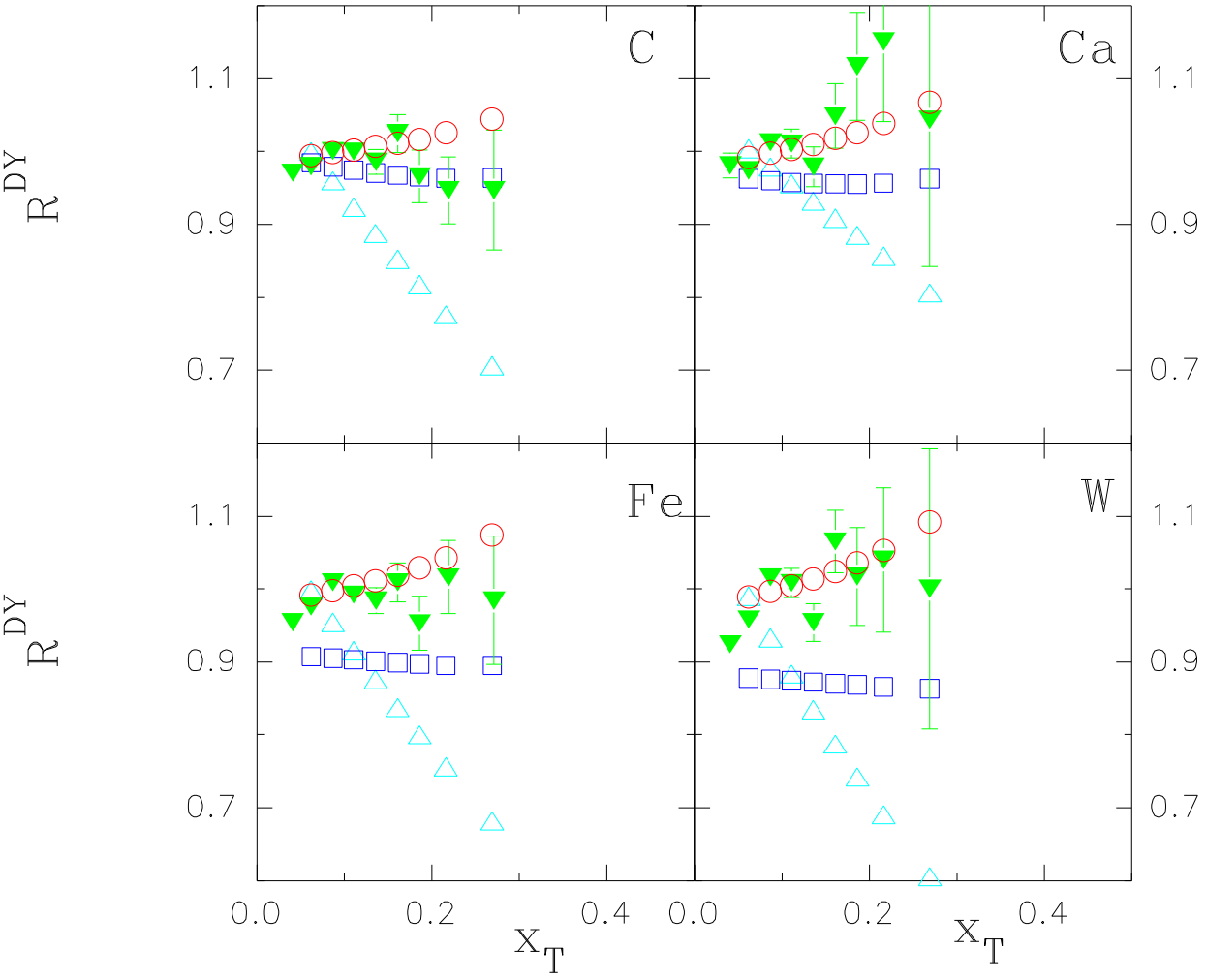

Figure 8